

A Digital Phantom for 3D MR Spectroscopy Data Simulation

D.M.J. van de Sande¹, A.T. Gudmundson^{2,3,4}, S. Murali-Manohar^{2,3}, C.W. Davies-Jenkins^{2,3}, D. Simicic^{2,3}, G. Simegn^{2,3}, İ. Özdemir^{2,3}, S. Amirrajab¹, J.P. Merkofer⁵, H.J. Zöllner^{2,3}, G. Oeltzschner^{2,3}, R.A.E. Edden^{2,3}

¹(Department of Biomedical Engineering, Eindhoven University of Technology, Eindhoven, The Netherlands)

²(Russell H. Morgan Department of Radiology and Radiological Science, The Johns Hopkins University School of Medicine, Baltimore, Maryland, USA)

³(F. M. Kirby Research Center for Functional Brain Imaging, Kennedy Krieger Institute, Baltimore, Maryland, USA)

⁴(The Malone Center for Engineering in Healthcare, Johns Hopkins University School of Engineering, Baltimore, Maryland, USA)

⁵(Department of Electrical Engineering, Eindhoven University of Technology, Eindhoven, The Netherlands)

Abstract

Purpose

Simulated data is increasingly valued by researchers for validating MRS and MRSI processing and analysis algorithms. However, there is no consensus on the optimal approaches for simulation models and parameters. This study introduces a novel 3D MRS digital brain phantom framework, providing a comprehensive and modular foundation for MRS and MRSI data simulation.

Methods

We generate a digital brain phantom by combining anatomical and tissue label information with metabolite data from the literature. This phantom contains all necessary information for simulating spectral data. We integrate the phantom with a signal-based model to demonstrate its functionality and usability in generating various spectral datasets. Outputs are saved in the NIfTI-MRS format, enabling their use in downstream applications.

Results

We successfully implemented and tested the 3D MRS digital brain phantom framework using two different anatomical models at two resolutions. The resulting metabolite maps and spectral datasets demonstrate realistic data quality, flexibility based on user inputs, and reasonable computational efficiency.

Conclusion

This innovative 3D digital brain phantom framework provides a clear and structured approach to simulating MRS and MRSI data. Its modular design establishes a strong, adaptable foundation for future advancements in MRS and MRSI simulation, allowing researchers to extend and refine the model to meet the field's evolving needs.

1 Introduction

Magnetic resonance spectroscopy (MRS) and spectroscopic imaging (MRSI) are powerful non-invasive techniques for measuring neurochemical concentrations in the human brain. These methods offer the potential to enhance our understanding of various neurological conditions by providing insights into the biochemical changes associated with disease processes^{1,2}. Despite their promise, the clinical implementation of MRS and MRSI has been hindered by several challenges, including time-consuming acquisition protocols, an inherently low signal-to-noise ratio (SNR), and the specialized expertise required for data processing and analysis³⁻⁵.

To address these challenges, researchers are actively developing innovative methodologies and toolboxes aimed at streamlining and standardizing the processing and analysis of MRS and MRSI data⁶⁻⁹. Additionally, the incorporation of machine learning techniques has emerged as a promising approach¹⁰⁻¹². However, the advancement of all these methodologies requires sufficient data for validation and algorithm testing. Access to MRS and MRSI datasets is often limited due to a lack of open-source databases and the high costs associated with data acquisition. Furthermore, in-vivo data typically does not provide ground-truth concentrations, which are crucial for accurately validating algorithms.

Consequently, simulating MRS and MRSI datasets is increasingly recognized as a valuable practice among researchers. Synthetic data generation not only allows for the creation of a vast number of spectra but also enables control over the ground-truth values associated with these spectra. Despite the widespread use of spectral simulation, there is no consensus on the optimal approaches for simulation models and parameters. The choices of signal model, parameter ranges, and validation of data realism are often intricate and diverse.

Within the field of MRI, numerous digital phantoms have been developed to simulate MR images¹³⁻¹⁶. These phantoms effectively combine anatomical information and tissue properties with physics-based models to produce realistic MR images. Such simulation tools have significantly advanced research in MRI image generation and analysis. To our knowledge, no digital phantom exists that is specifically designed to generate MRS and MRSI data by integrating anatomical information with current knowledge of brain metabolites. Therefore, the purpose of this work is to develop a novel simulation framework for generating MRS and MRSI data using a 3D MRS digital brain phantom. Our framework will focus on integrating anatomical brain information with established literature regarding brain metabolite concentrations and relaxation times. The 3D MRS digital brain phantom framework will provide a comprehensive and modular foundation tool for creating a data generation pipeline, allowing for the adaptation or replacement of various modules as needed. The resulting framework is available as an open-source tool written in Python, facilitating further research and development in the field (<https://github.com/dennisvds/MRS-Digital-Phantom>).

2 Materials & Methods

The overall outline of our proposed 3D MRS digital brain phantom framework is shown in Figure 1. This structure is divided into three stages: skeleton, MRS phantom, and simulation. All computational tasks were performed using a MacBook Pro with M2 Pro chip (10 core CPU/16 core GPU) and equipped with 16GB of RAM.

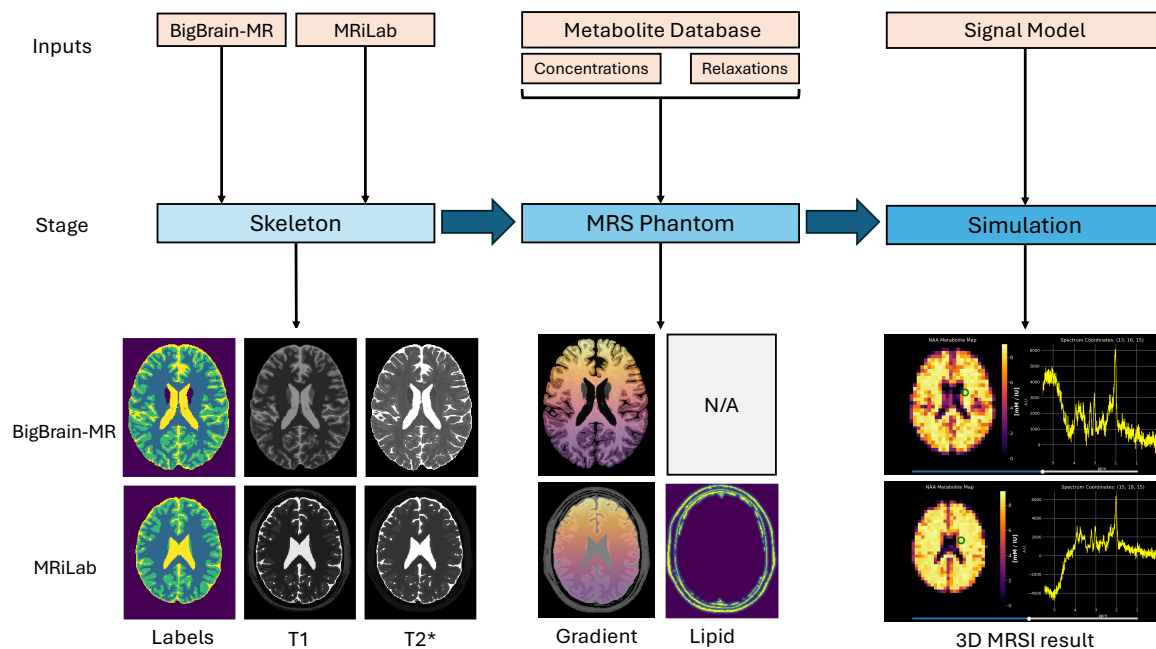


Figure 1: Structure of the 3D MRS digital brain phantom framework. The framework is divided into three stages: Skeleton, MRS Phantom, and Simulation. Each stage allows for user-defined inputs, making the framework highly modular and customizable for various applications.

2.1 Skeleton

The anatomical information of the proposed framework is a three-dimensional brain phantom, referred to as the skeleton. This skeleton provides information about the anatomy and tissue labels of the MRS phantom. Additionally, other maps (e.g. relaxation and field inhomogeneity maps) can be loaded to provide more MR related properties. For this study, we integrate two different sources of brain anatomical phantoms: BigBrain-MR and the MRiLab phantom.

BigBrain-MR is a three-dimensional brain phantom with up to $100 \mu\text{m}$ resolution¹⁶. It is created by combining a low-resolution MRI acquired at 7T with a high-resolution histological dataset to create an in-vivo-like high-resolution tissue property map. The tissue label map, T_1 map, R_2^* map, and T_1 -weighted image are used for this study. The BigBrain-MR phantom contains 20 distinct labels, however, only those voxels designated as white matter (WM), gray matter (GM), or cerebrospinal fluid (CSF) are used in the framework, while the remaining voxels are set to the background label. The R_2^* map is transformed into a T_2^* map and both the T_1 and T_2^* maps are converted into seconds. Since the T_1 and T_2^* maps are still based on 7T data, a scaling is applied on these maps to create 3T equivalents. The scaling factors to transform the T_1 maps are based values found in literature¹⁷ and are $S_{T_1,WM} = 0.723$, $S_{T_1,GM} = 0.727$, $S_{T_1,CSF} = 1$ with $S_{T_1,WM}$, $S_{T_1,GM}$, and $S_{T_1,CSF}$ the scaling factors for WM, GM, and CSF respectively.

Scaling for the T_2^* maps is done by assuming a linear dependence between $1/T_2^*$ and the field strength B_0 .

The MRiLab phantom is sourced from a MATLAB-based numerical MRI simulation package called MRiLab¹³. It contains a three-dimensional tissue label map at 1 mm resolution and corresponding T_1 , T_2 , T_2^* , and proton density (PD) maps for which the values are based on literature studies. In contrast to the BigBrain-MR phantom, this phantom contains voxels with information about the skull and its neighboring lipids. This information allows the creation of lipid maps (see Section 2.2.2) that can be utilized for simulating lipid contamination for realistic MRS generation.

All phantom maps for both BigBrain-MR and MRiLab, are saved and loaded using the NIfTI file format¹⁸. For further use in the MRS phantom, all maps are resampled to either a 1 mm or 3 mm resolution using the TorchIO library¹⁹.

2.2 MRS Phantom

2.2.1 Metabolite Database

In the second stage, metabolite information is combined with the skeleton. In this study, metabolite concentrations and T_2 values for WM and GM are extracted from an open-source database of a previously published meta-analysis²⁰. This database summarizes nearly 500 studies that report metabolite relaxations and concentrations for the healthy human brain and for various pathologies. For this study, the database is filtered according to Figure 2. All studies are filtered on healthy and control patients and are only included when information about GM and WM fractions is present. Since the phantom uses binary tissue labels, metabolite concentrations are assigned to GM or WM based on tissue fractions: regions with a tissue fraction of 0.6 or higher are categorized as belonging to that tissue type. Next, all studies are filtered on the age range of 18 to 60 years old, and the metabolite nomenclature is checked and homogenized. The metabolite concentrations for tCr, tNAA, tCho, and Glx are split into their individual components based on known relations found in literature^{21,22} and the concentration data in units of mM and IU are combined similarly as in the meta-analysis. The T_2 database is filtered on studies that use 3T scanners. Finally, metabolite concentrations and T_2 values are calculated using a random effects model²³, with weights determined by the inverse square of the reported standard deviations. If only one study is available for a specific tissue-metabolite combination, the values reported in this study are used.

When all metabolite concentrations and T_2 relaxation times are calculated, the results are saved in a metabolite dataframe format that is integrated into the MRS phantom. It ensures compatibility with the MRS phantom, but also allows the user to choose their own metabolite concentrations and relaxation times within this specified format. Since the meta-analysis did not contain any information about CSF labelled voxels, metabolite information about these voxels is manually added in the metabolite dataframe based on other literature values²⁴. A placeholder for metabolite T_1 relaxation has also been built in for future updates. The current framework also requires

background labels, for which all metabolite information is automatically set to zero. An example of this metabolite dataframe format is shown in Supporting Information Table S1.

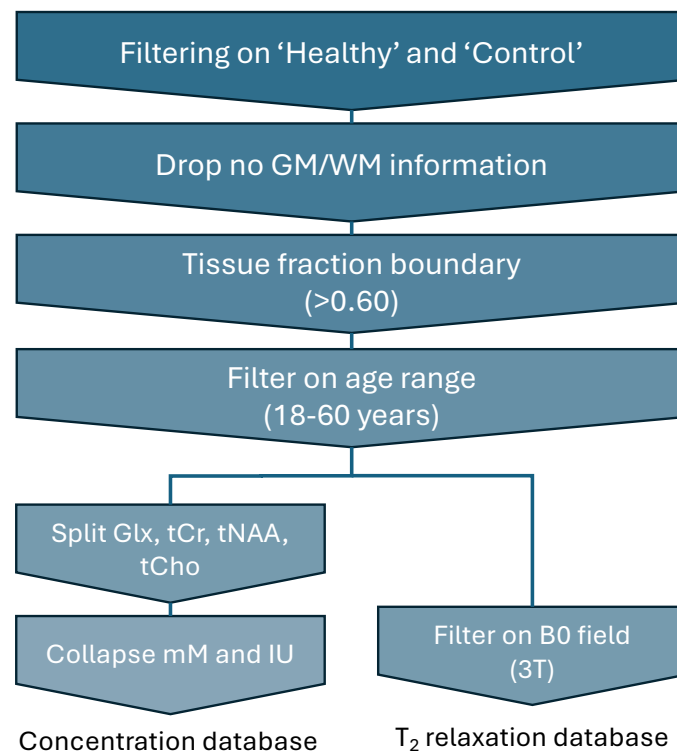


Figure 2: Filtering flowchart of the metabolite database entries used. These steps are performed to select the appropriate subset of entries collected in the previous meta-analysis.

2.2.2 Phantom Class

The metabolite database and the skeleton are combined to form the MRS phantom, which represents the primary structural element of our proposed framework. The MRS phantom is a Python class object designated '*DigitalPhantom*', which comprises several attributes, as detailed in Table 1. These attributes are classified into three categories: user inputs, class variables, and class methods. User inputs influence the characteristics of the MRS phantom during its creation and loading. Class variables are stored within the MRS phantom and contain parameters and information pertaining to the MRS phantom. Class methods process the MRS phantom data and return data for subsequent applications.

Table 1: Overview of MRS Digital Phantom attributes.

User Inputs	Type	Description
skeleton	string	The name of the skeleton to use for the phantom ('BigBrainMR' or 'MRiLab').
phantom_resolution	float	Resolution of the phantom in mm.
path2skeleton	string	The path to the skeleton data.
path2phantom	string	The path to save and load the MRS phantom data.

path2metabs	string	The path to the metabolite dataframe.
from_scratch	Boolean	Whether to create the phantom from scratch, even if saved files can be loaded.
concs_std	float	The standard deviation of the metabolite concentrations given as a percentage of the mean. If None, the standard deviation from the metabolite dataframe is used.
sigma_lipid_spread	float	Sigma value for Gaussian blur to control lipid contamination in the brain.
grad_settings	list [float, float, string]	Settings for the metabolite concentration gradients: [minimum gradient map value, maximum gradient map value, gradient direction]. The gradient direction can be set to '+x', '+y', '+z', '-x', '-y', and '-z'. The gradient is multiplied with the concentration.
grad_metabs	list of strings	List of metabolites on which the gradient map is applied

Class Variables	Type	Description
subject	TorchIO subject	Phantom subject object which holds all phantom maps
affine	numpy.ndarray	Affine matrix for all MRS phantom maps
lipid_map	numpy.ndarray	Map that represents the amount of lipid contamination in every voxel
metab_data	numpy.ndarray	Array that contains all voxels and their metabolite information (the metabolite data matrix).
dim_info	dict	Dictionary with the used dimensions in 'metab_data'
metab_dim_info	dict	Dictionary with the used dimensions in the metabolite_info dimension of the 'metab_data' array.
metab_mapping	dict	Dictionary with metabolite ID's and their corresponding names

Class Methods	Output Type	Description
get_phantom_info	None	Prints properties of the current loaded MRS Phantom.
create_metab_map	numpy.ndarray	Method to extract a 3D metabolite concentration map from the MRS phantom.

extract_sim_data	numpy.ndarray, list of strings	Method to extract metabolite data needed for spectral simulations.
-------------------------	-----------------------------------	---

The core class variable in the *DigitalPhantom* class is the metabolite data matrix, which is named *'metab_data'* (see Table 2). This data matrix contains metabolite information on a voxel level and gives information about the mean and standard deviations of the concentrations and the relaxation times of each individual metabolite. This matrix is the result of combining the label information from the skeleton with the metabolite database. Actual concentration values are set using the mean and standard deviations in the metabolite data matrix or, if the *'concs_std'* user input is provided, by taking the mean and using the standard deviation from the user input.

Spatial variations can also be included during the creation of the metabolite data matrix. Since the literature database used does not have detailed information about the spatial dependency of the concentrations, artificial gradient maps are included as a proof of concept. We create a linear gradient map across the brain that is multiplied with the metabolite concentrations in the data matrix to include spatial variations to the metabolite concentration, depending on the location of the brain. The direction and strength of these gradients can be adjusted by the user using the *'grad_settings'* input. This input enables the user to set a direction and a minimum and maximum value of the gradient map. The metabolite concentrations, specified in *'grad_metabs'*, are then multiplied with this artificial gradient map. Figure 3 shows a metabolite map of NAA with and without the artificial gradient applied.

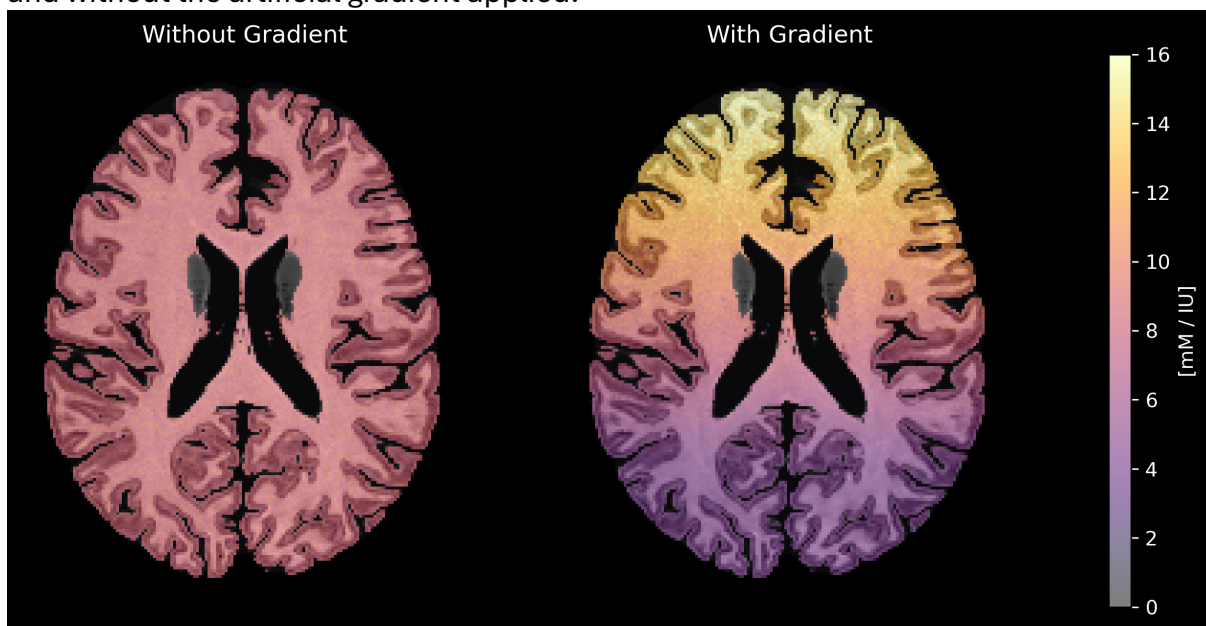


Figure 3: Axial slice of an NAA map with and without an applied concentration gradient. This example uses the BigBrain-MR skeleton and applies a gradient with *'grad_settings'* of [0.5, 2.0, '+y']. This results in a linear gradient from 0.5 to 2.0 along the positive y-axis, which is then multiplied with the NAA map.

If information about lipid voxels is present in the skeleton, the *DigitalPhantom* class will also generate lipid maps. These maps represent the amount of lipid contamination throughout the MRS phantom, which is a combination of the predicted physiological presence of lipid and the point-spread function (PSF) from those locations due to imperfect imaging or localization. First, a binary mask is created which contains all lipid

voxels. To model the spread of the lipid signal, a Gaussian filter is applied to the binary lipid mask that acts as the PSF. The resulting map is then normalized to maintain interpretability, as it adjusts the map by scaling the highest lipid contaminated voxel to a value of one and gradually decrease the surrounding voxels towards zero. The standard deviation of the Gaussian filter, and thus the amount of lipid contamination in voxels further away from the lipid labels, is part of the user inputs (see ‘*sigma_lipid_spread*’). The lipid map creation is visualized in Figure 4.

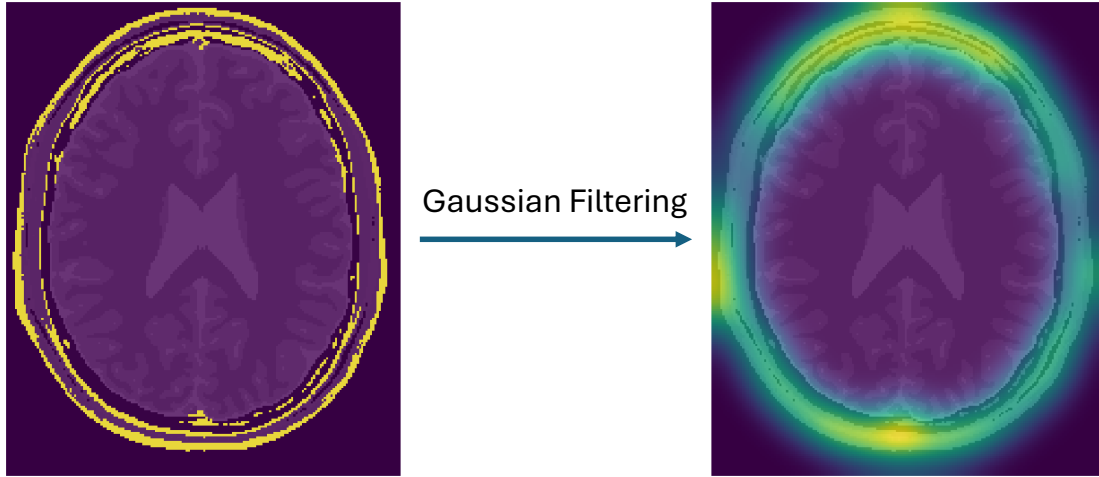


Figure 4: Axial slice of the MRiLab phantom showing the creation of a lipid map. A binary lipid mask is blurred by using a Gaussian filter to mimic the point-spread function (PSF). For this example, the sigma of this lipid spread was set to 8.0.

2.3 Signal Model

To show the functionality of the MRS phantom framework, a MRS signal model is implemented that generates MRS(I) data based on the digital phantom. This signal model is based on the Voigt forward model from FSL-MRS⁷, adapted to a batch-wise implementation to allow efficient signal generation for multiple voxels. The simulation procedure can be broken down into different modules: metabolite simulation, macromolecule (MM) simulation, water simulation, and lipid simulation. Spectra are generated voxel-by-voxel at the resolution of the MRS phantom. The user can define which metabolites need to be included and which slices (in the z-dimension) should be simulated.

2.3.1 Metabolite Simulation

For generating a metabolite spectrum in the frequency domain, $Y(\nu)$, the following signal model is used:

$$Y(\nu) = \sum_{n=1}^M C_n M_n(\nu, \epsilon_n, \gamma_n, \sigma_n)$$

with

$$M_n(\nu, \epsilon_n, \gamma_n, \sigma_n) = FFT\{m_n(t) \exp [(-i\epsilon_n - \gamma_n - \sigma_n^2 t)t]\}$$

where for each metabolite n , we define a metabolite concentration (C_n), a basis spectrum in the time domain ($m_n(t)$), a frequency shift (ϵ_n), a Lorentzian decay factor

(γ_n), a Gaussian decay factor (σ_n). Values for C_n and γ_n are extracted per voxel from the MRS phantom, where γ_n is based on the metabolite T_2 values ($\gamma = 1/(\pi T_2)$). The basis set is left as a user input and can be changed with every simulation. Currently, the simulation model can implement Osprey and LCMModel basis set formats. Finally, ϵ_n and σ_n are left as user inputs that can be defined before every simulation.

2.3.2 Macromolecule Simulation

The MM background is simulated based on the approach used in the work of Wright et al.²⁵. This method generates Voigt line shapes for a set of predefined MM resonances. Information about T_1 , T_2 , linewidths, and relative scaling factors are taken from the literature²⁶⁻²⁸. By using known linewidths and T_2 values of the MMs, the Lorentzian and Gaussian components of the MM line shapes can be determined.

2.3.3 Residual Water Simulation

Residual water signal is added by performing a random walk within a specified frequency range (4.4-5.5 ppm). This random walk starts within specified y-axis limits and every next value is drawn from a normal distribution with a specified standard deviation. To make the signal more realistic and deal with sharp edges at the frequency limits, the random walk is smoothed by convolution. The obtained real signal is converted to the complex domain by using the Hilbert transform and scaled to fit the amplitudes of the metabolites. All settings for the residual water signal are empirically set and can be changed by the user. An example of such random walks is visualized in Figure 5.

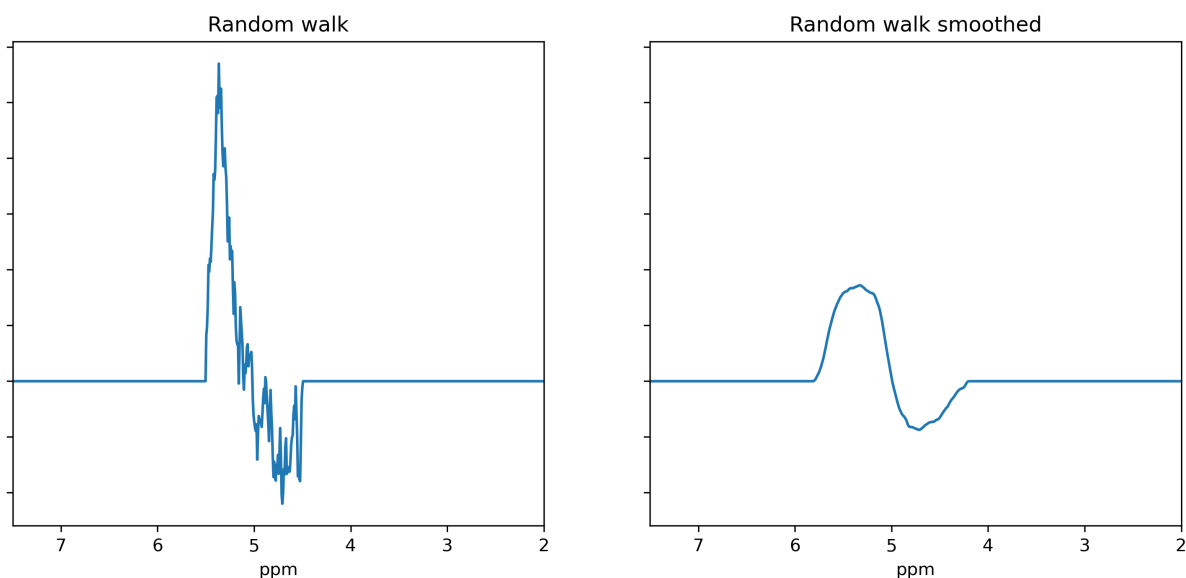


Figure 5: Graphical representation of a random walk that is used to generate residual water signals. The random walk is smoothed using a convolution kernel.

2.3.4 Lipid Simulation

To include lipid contamination, expected frequency values, widths, and amplitude ratios are extracted from the LCModel manual²⁹. By using these parameters, 6 random peaks are generated, all between 0.89 and 2.04 ppm. The first order phasing (ϕ_0) of the peaks is randomized by using a uniform distribution ($-\pi \leq \phi_0 \leq \pi$) and the imaginary part of the signal is obtained by using the Hilbert transform. The generated lipid peaks are summed, and the resulting spectrum is multiplied with the lipid map from the MRS phantom. An additional scaling factor is left as a user input to control the level of overall lipid contamination.

2.3.5 Baseline and Noise

A baseline is incorporated into the spectra following the complex polynomial baseline model used in FSL-MRS⁷. Users can specify the baseline order and a scaling factor. Based on these inputs, a complex baseline is generated, scaled accordingly, and then applied to all spectra. Additionally, Gaussian noise is introduced, with its standard deviation adjustable through a user-defined input.

2.3.6 Simulation Outputs

All spectra are generated on the resolution of the MRS phantom, which can be as small as 1 mm. However, during typical MRSI acquisitions at 3T voxel sizes range from 3 to 10 mm. Therefore, a downsampling method is developed to reduce the spatial resolution while maintaining the key spectroscopic information. This method takes the high-resolution MRSI data and applies average pooling to reduce the spatial resolution. The method calculates the ratio between the target and original resolutions to define a block size, which determines the number of neighboring voxels that will be pooled together. The pooling of the data is implemented by traversing the 3D space of the original MRSI data and averaging voxel values within each block, computed based on the block size. For each voxel in the reduced resolution space, a window is extracted from the original data. The average intensity across this window is calculated and stored in the corresponding position of the reduced data array.

All simulation results are saved in the NIfTI-MRS data format³⁰. By using this format, simulated data can be exported and used in software development or machine learning models for downstream applications. To enhance usability and ensure reproducibility, default parameter values for the entire simulation pipeline are made available in the code repository. These values are outlined in the relevant functions and are also included in the demonstration notebook, allowing users to easily understand and adapt the simulation process to their needs.

3 Results

3.1 MRS Phantom

Filtering of the metabolite database resulted in a metabolite concentration dataframe with 783 entries, consisting of 54 unique references and including 19 unique

metabolites. For the T_2 relaxation times, 219 entries are available after filtering with 18 references and 19 metabolites. All these entries are used to determine the metabolite information in the MRS phantom. For some metabolites, information was missing that caused missing values for GM and/or WM in terms of concentrations and T_2 relaxation.

Examples of metabolite maps are shown in Figure 6. These maps can be seen as ground truth metabolite maps that are stored in the MRS phantom. Since the metabolite database is focusing on different tissue types, the biggest concentration differences can be seen when comparing GM and WM. Other variations are caused by the predefined standard deviation of the concentrations.

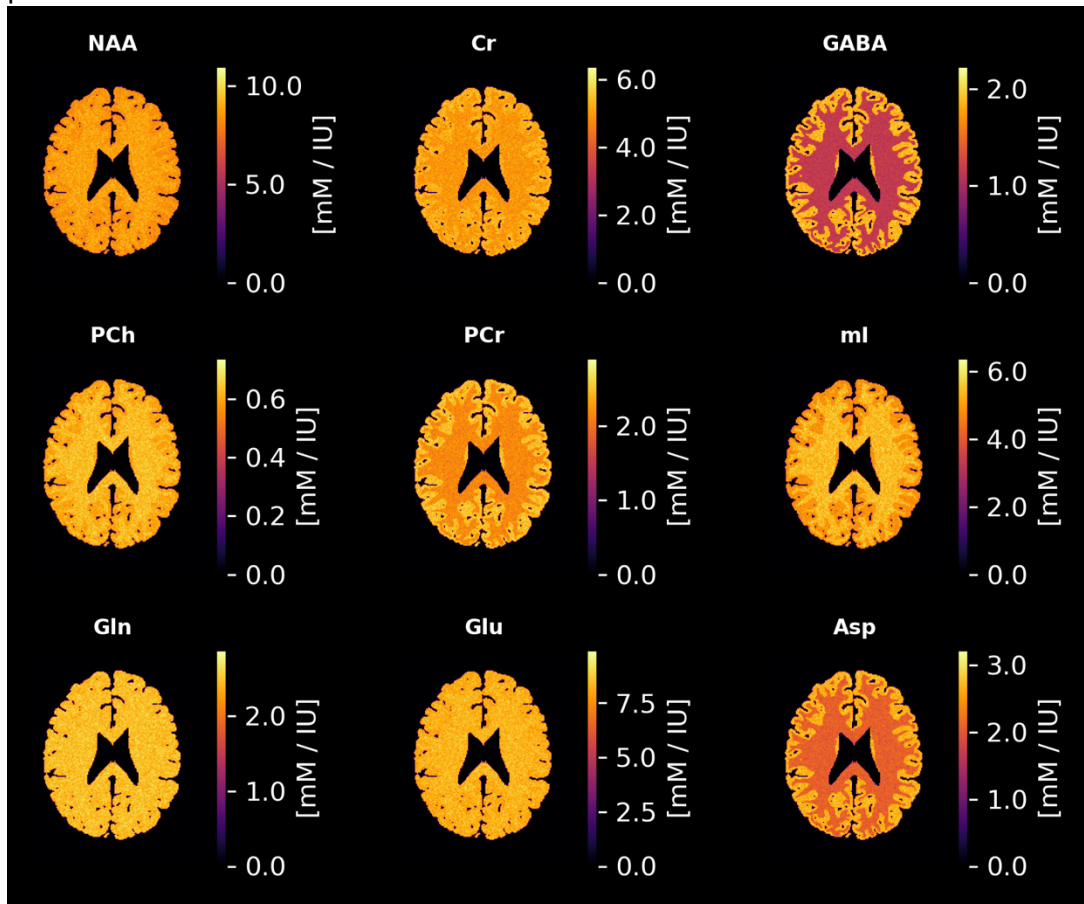


Figure 6: Metabolite maps generated by the MRS phantom. This is the result of combining the skeleton (BigBrain-MR, 1mm resolution) with the metabolite database. The standard deviation is set to 5% of the mean concentrations.

3.2 Signal Model

The signal model, outlined in Section 2.3, evaluates the usability of the MRS phantom. Figure 7 illustrates examples of generated spectra, showing gradual changes in parameters that control the spread of lipid contaminations, Gaussian line broadening, and noise standard deviation, while keeping all other parameters constant. All these spectra derive from the same MRS phantom and voxel location. This demonstration highlights the high modularity and flexibility of the MRS phantom when combined with the signal-based model.

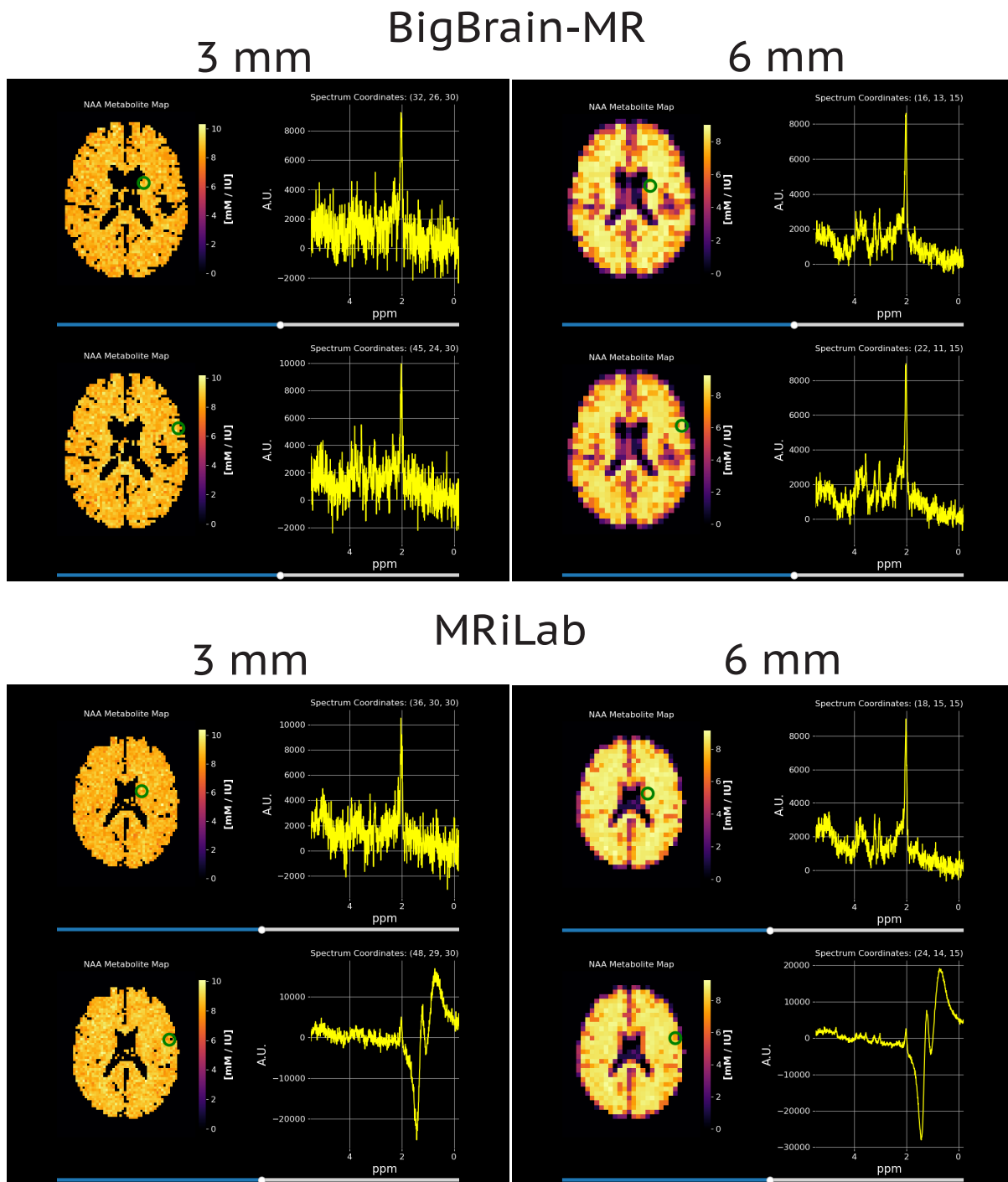


Figure 8 presents data for both skeletons generated at 3 mm isotropic resolution and the downsampled data at a 6 mm resolution. Spectra from two distinct voxel locations highlight the variations between the datasets, including the presence of lipid contamination in the MRiLab skeleton near the skull. This figure shows that the SNR improves for the downsampled data, as this downsampling uses a custom averaging pooling method discussed in Section 2.3.6.

Figure 9 shows an example of exported MRSI data, visualized using FSLeaves³¹. This data, generated using the proposed 3D MRS digital phantom framework, employs the MRiLab

skeleton at a 3 mm isotropic resolution. Data is generated for all slices. Subsequently, the resulting MRSI map is downsampled to a 6 mm isotropic resolution.

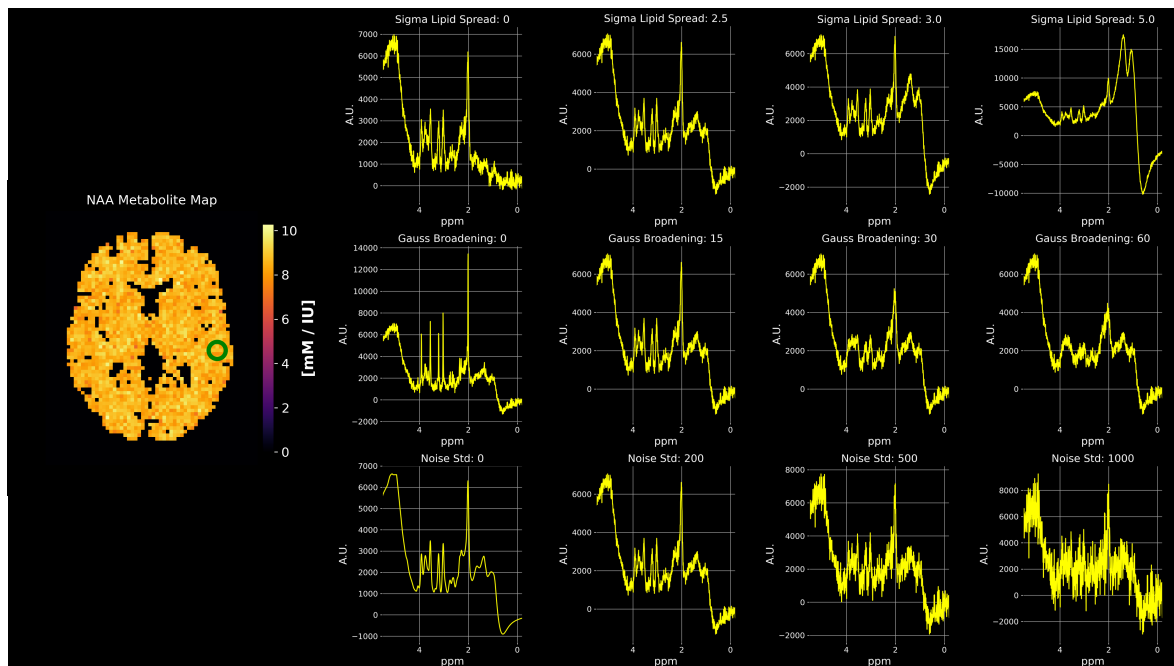


Figure 7: Examples of generated spectra using the MRS phantom framework. On the left, the NAA metabolite map is shown with a marker that indicates the voxel location of the generated spectra. Variations in the spread of lipid contaminations, Gaussian line broadening, and noise standard deviation are shown in the top, middle, and bottom rows respectively.

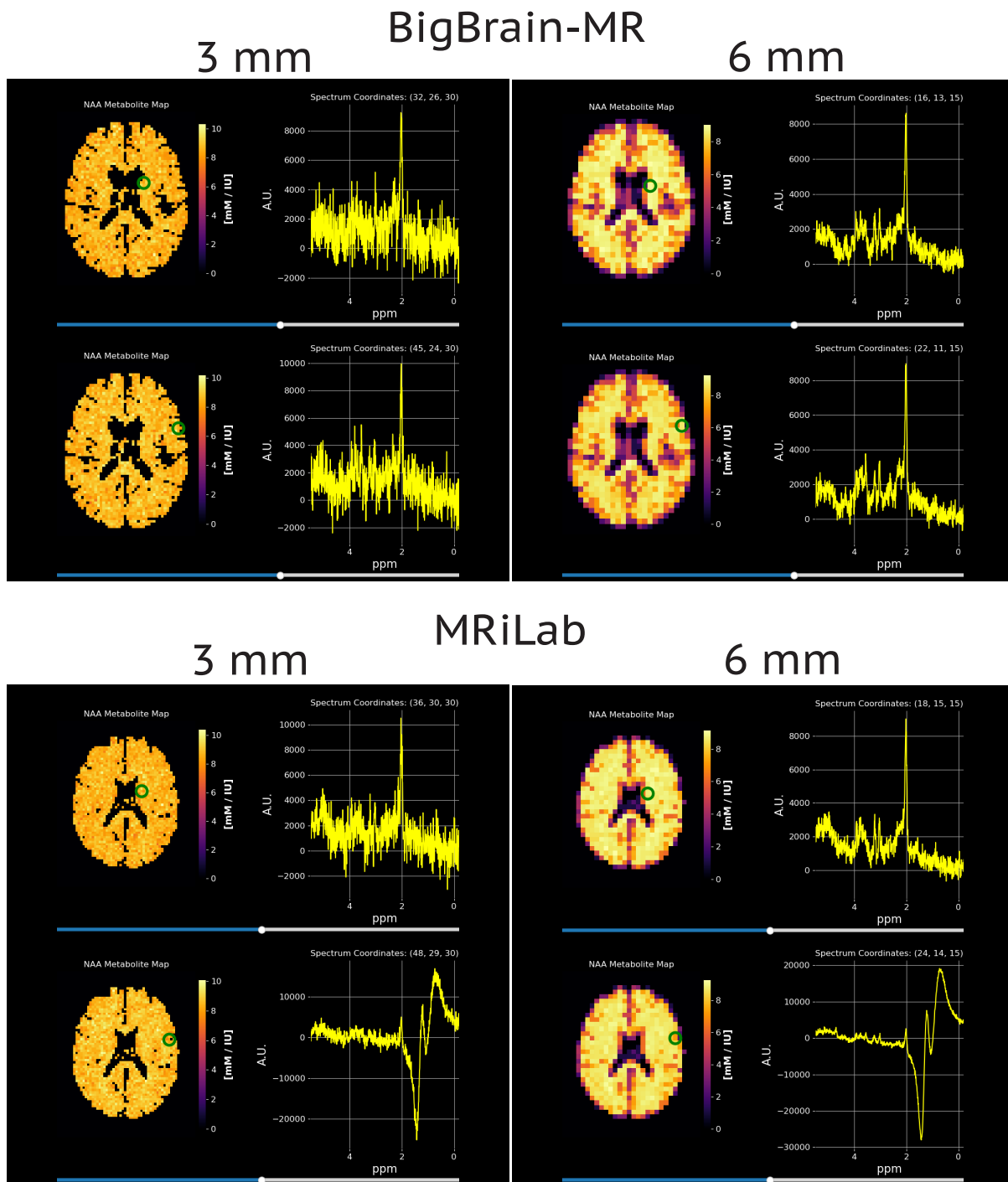


Figure 8: Simulation results of the MRS phantom. The left column presents NAA metabolite maps and spectra at 3 mm resolution, while the right column displays them at 6 mm resolution. The top four panels use the BigBrain-MR skeleton, and the bottom four use the MRiLab skeleton. The green cross marks the voxel location for the displayed spectrum. Notably, the MRiLab skeleton generates lipid signals near the skull, distinguishing it from the BigBrain-MR skeleton.

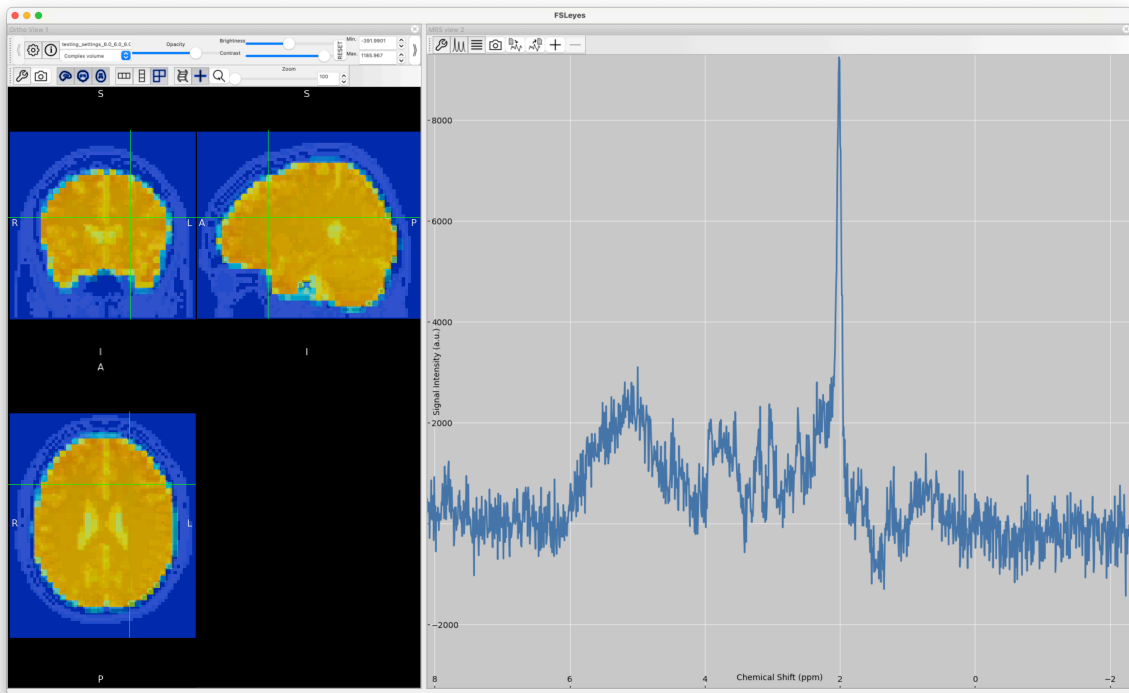


Figure 9: Screenshot of the MRS phantom and its generated data loaded into FSLeaves³¹. The data is simulated using the MRiLab skeleton at a 3 mm isotropic resolution for all slice numbers, and then downsampled to a 6 mm resolution.

3.3 Computation times

The computation times for all steps in the 3D MRS brain phantom framework were analyzed for both the BigBrain-MR and MRiLab skeletons at 1 mm and 3 mm isotropic resolutions. Filtering the database was computationally lightweight, requiring only a few seconds. Generating the phantom from scratch required significantly more computation time at 1 mm resolution compared to 3 mm resolution. However, replacing this step with loading pre-generated NIfTI files reduced computation times to just a few seconds for both resolutions. Spectral simulation for all slices was the most time-intensive step, with computation times increasing proportionally to the number of spectra generated—substantially higher for the 1 mm resolution due to its larger data size. Finally, the downsampling process, which converts the simulated data to lower isotropic resolutions and saves them as NIfTI-MRS files, also required significantly more time at 1 mm resolution than at 3 mm resolution. Detailed timing data for each step is provided in the Supporting Information Table S2.

4 Discussion

The proposed digital MRS phantom framework provides a modular and comprehensive tool for simulating MRS and MRSI data. By integrating tissue-dependent metabolite information with a signal-based simulation model, it generates realistic MRS(I) datasets according to user-defined settings. Using a filtered metabolite database, the framework incorporates prior knowledge of metabolite concentrations to create detailed brain

metabolite maps. Saving the generated data in the NIfTI-MRS format ensures compatibility with a wide range of downstream applications.

4.1 MRS Phantom

This framework has been tested with two anatomical templates: the BigBrain-MR and the MRiLab phantom. These templates serve as an excellent foundation for producing simple MRSI datasets for benchmarking purposes. The framework's modularity facilitates future expansion to include diverse anatomical models, enhancing its versatility. An optimized approach for managing multiple anatomical models efficiently would further extend its applicability. Additionally, integrating a registration method would align information across different anatomical skeletons, improving dataset consistency. For example, registering skull or lipid voxels from one template to another would standardize key features, like lipid map creation, across datasets.

The metabolite dataframe currently used is based on a subset of a larger database from a separate meta-analysis. As shown in Figure 2, this approach carefully balances the need for homogeneity with the inclusion of sufficient studies to produce meaningful averages. While summarizing data from heterogeneous sources poses challenges, the framework remains flexible. It enables adjustments to the mean and standard deviation of each metabolite concentration, thereby enabling the simulation of pathological conditions. Expanding the framework to include metabolite data for different patient cohorts and tissue types would significantly enhance its applicability and clinical relevance.

Currently, the framework does not account for spatial variability in metabolite concentrations within brain regions, despite evidence indicating such heterogeneity exists^{24,32,33}. Including such variability would enhance the utility of the framework for investigating localized metabolic differences and disease-specific alterations. The gradient maps, currently included in the framework, already demonstrate its potential for incorporating spatially dependent metabolite distributions. Implementing this capability would greatly improve the biological realism of the simulated datasets.

Another potential improvement involves the addition of detailed information regarding acquisition settings, which play a critical role in generating the synthetic spectra. Factors such as pulse sequences, B_0 inhomogeneity, and the presence of outer-volume suppression (OVS) significantly influence the spectral output in both MRS and MRSI acquisitions. While the framework is designed to accommodate these parameters, their full implementation and rigorous testing remain necessary to elevate the quality and relevance of synthetic datasets.

4.2 Signal Model

The signal model used for the simulations integrates well with the overall MRS phantom framework, providing a solid foundation for generating realistic MRS and MRSI data. However, several areas of improvement could enhance the model's ability to more accurately replicate real-world acquisition conditions.

The current approach to lipid signal modeling, where signals are fixed per simulation run and scaled uniformly via the lipid map, serves basic simulation purposes well. However, integrating spatial variability and tissue-specific characteristics would offer greater flexibility. A similar approach could be taken for MM signals, which are presently fixed and scaled uniformly across voxels. Implementing a more flexible parameterized model for MM signals would enable more precise representations of their variability across different brain regions and tissue types, enhancing the realism of the simulated datasets.

The inclusion of artifacts such as chemical shift displacement error (CSDE) could substantially elevate the utility of the framework. This artifact results from the spatial misregistration of metabolites due to differences in chemical shift frequencies. Including the simulation of such artifacts would enhance the model's utility for evaluating methods aimed at mitigating these issues in real MRSI datasets.

The current down sampling method works well to lower the resolution of the generated MRSI data, but it is not mimicking real-world acquisition techniques. Future developments can focus on how to implement specific MRSI acquisition schemes into the simulation framework and on generating k-space data to set desired resolutions using various ways of (under)sampling.

4.3 Computation and Accessibility

The current implementation of the 3D MRS digital brain phantom framework requires a couple of minutes to generate an MRSI dataset of the full brain at 3 mm resolution, while simulations at 1 mm resolution can take up to 42 minutes (see Supporting Information Table S2). These findings highlight the computational demands of high-resolution simulations. Future efforts focused on optimizing computational efficiency, such as the implementation of multiprocessing and parallel processing techniques, will be crucial for reducing computation times. Such improvements will enable the generation of large numbers of datasets more efficiently, supporting applications that require extensive MRSI data simulation for research and clinical purposes.

Finally, while the current demonstration notebook provides guidance for users, a graphical user interface (GUI) would enhance the accessibility of the framework. A user-friendly interface would facilitate the customization of modules, making the tool more approachable for researchers with limited programming experience. This would broaden the reach and application of the framework, promoting its use in diverse research settings and facilitating collaboration.

The digital MRS phantom framework serves as a comprehensive and user-friendly resource, effectively bridging the gap between simulation and clinical practice while supporting advancements in MRS data analysis and methodology. Its modular and flexible design enhances adaptability and encourages users to integrate their own improvements. This open approach invites the research community to build upon the existing framework, fostering collaboration and innovation to continually refine and expand its capabilities.

5 Conclusion

This work introduces an innovative framework for simulating MRS and MRSI data through a 3D digital brain phantom. By integrating anatomical and metabolic data with a signal-based simulation model, the framework produces realistic and detailed spectral datasets. While there is room for further improvement through the incorporation of more advanced algorithms, the framework's modular design establishes a strong and adaptable foundation for the continued advancement of MRS and MRSI simulation. Its flexibility supports future development, empowering researchers to extend and refine the model to meet evolving needs in the field.

6 Acknowledgements

We would like to thank the Fulbright Commission the Netherlands for financially supporting the visit of D.M.J. van de Sande to The Johns Hopkins University School of Medicine, Baltimore, USA. This research was performed in the Spectralligence project, funded by the European ITEA4 program (project 20209).

7 References

1. Faghihi R, Zeinali-Rafsanjani B, Mosleh-Shirazi MA, et al. Magnetic Resonance Spectroscopy and its Clinical Applications: A Review. *J Med Imaging Radiat Sci.* 2017;48(3):233-253. doi:10.1016/j.jmir.2017.06.004
2. Öz G, Alger JR, Barker PB, et al. Clinical Proton MR Spectroscopy in Central Nervous System Disorders. *Radiology.* 2014;270(3):658-679. doi:10.1148/radiol.13130531
3. Near J, Harris AD, Juchem C, et al. Preprocessing, analysis and quantification in single-voxel magnetic resonance spectroscopy: experts' consensus recommendations. *NMR Biomed.* 2021;34(5):e4257. doi:10.1002/nbm.4257
4. Maudsley AA, Andronesi OC, Barker PB, et al. Advanced magnetic resonance spectroscopic neuroimaging: Experts' consensus recommendations. *NMR Biomed.* 2021;34(5):e4309. doi:10.1002/nbm.4309
5. Kreis R, Boer V, Choi IY, et al. Terminology and concepts for the characterization of in vivo MR spectroscopy methods and MR spectra: Background and experts' consensus recommendations. *NMR Biomed.* 2021;34(5):e4347. doi:10.1002/nbm.4347
6. Oeltzschner G, Zöllner HJ, Hui SCN, et al. Osprey: Open-source processing, reconstruction & estimation of magnetic resonance spectroscopy data. *J Neurosci Methods.* 2020;343:108827. doi:10.1016/j.jneumeth.2020.108827
7. Clarke WT, Stagg CJ, Jbabdi S. FSL-MRS: An end-to-end spectroscopy analysis package. *Magn Reson Med.* 2021;85(6):2950-2964. doi:10.1002/mrm.28630

8. Simpson R, Devenyi GA, Jezzard P, Hennessy TJ, Near J. Advanced processing and simulation of MRS data using the FID appliance (FID-A)—An open source, MATLAB-based toolkit. *Magn Reson Med*. 2017;77(1):23-33. doi:10.1002/mrm.26091
9. Gajdošík M, Landheer K, Swanberg KM, Juchem C. INSPECTOR: free software for magnetic resonance spectroscopy data inspection, processing, simulation and analysis. *Sci Rep*. 2021;11(1):2094. doi:10.1038/s41598-021-81193-9
10. Chen D, Wang Z, Guo D, Orekhov V, Qu X. Review and Prospect: Deep Learning in Nuclear Magnetic Resonance Spectroscopy. *Chem – Eur J*. 2020;26(46):10391-10401. doi:10.1002/chem.202000246
11. Rajeev SK, Rajasekaran MP, Krishna Priya R, Al Bimani A. A Review on Magnetic Resonance Spectroscopy for Clinical Diagnosis of Brain Tumour using Deep Learning. In: *2021 3rd International Conference on Advances in Computing, Communication Control and Networking (ICAC3N)*. ; 2021:461-465. doi:10.1109/ICAC3N53548.2021.9725561
12. van de Sande DMJ, Merkofer JP, Amirrajab S, et al. A review of machine learning applications for the proton MR spectroscopy workflow. *Magn Reson Med*. 2023;90(4):1253-1270. doi:10.1002/mrm.29793
13. Liu F, Velikina JV, Block WF, Kijowski R, Samsonov AA. Fast Realistic MRI Simulations Based on Generalized Multi-Pool Exchange Tissue Model. *IEEE Trans Med Imaging*. 2017;36(2):527-537. doi:10.1109/TMI.2016.2620961
14. C T, C L, Lr S, Fg Z. VirtMRI: A Tool for Teaching MRI. *J Med Syst*. 2023;47(1). doi:10.1007/s10916-023-02004-4
15. Stöcker T, Vahedipour K, Pflugfelder D, Shah NJ. High-performance computing MRI simulations. *Magn Reson Med*. 2010;64(1):186-193. doi:10.1002/mrm.22406
16. Sainz Martinez C, Bach Cuadra M, Jorge J. BigBrain-MR: a new digital phantom with anatomically-realistic magnetic resonance properties at 100- μ m resolution for magnetic resonance methods development. *NeuroImage*. 2023;273:120074. doi:10.1016/j.neuroimage.2023.120074
17. Rooney WD, Johnson G, Li X, et al. Magnetic field and tissue dependencies of human brain longitudinal $1\text{H}_2\text{O}$ relaxation in vivo. *Magn Reson Med*. 2007;57(2):308-318. doi:10.1002/mrm.21122
18. Cox RW, Ashburner J, Breman H, et al. A (sort of) new image data format standard: NiFTI-1. In: Vol 22. 10th Annual Meeting of the Organization for Human Brain Mapping. ; 2004.
19. Pérez-García F, Sparks R, Ourselin S. TorchIO: A Python library for efficient loading, preprocessing, augmentation and patch-based sampling of medical images in deep learning. *Comput Methods Programs Biomed*. 2021;208:106236. doi:10.1016/j.cmpb.2021.106236

20. Gudmundson AT, Koo A, Virovka A, et al. Meta-analysis and open-source database for in vivo brain Magnetic Resonance spectroscopy in health and disease. *Anal Biochem.* 2023;676:115227. doi:10.1016/j.ab.2023.115227
21. Govindaraju V, Young K, Maudsley AA. Proton NMR chemical shifts and coupling constants for brain metabolites. *NMR Biomed.* 2000;13(3):129-153. doi:10.1002/1099-1492(200005)13:3<129::AID-NBM619>3.0.CO;2-V
22. Pouwels PJW, Frahm J. Differential distribution of NAA and NAAG in human brain as determined by quantitative localized proton MRS. *NMR Biomed.* 1997;10(2):73-78. doi:10.1002/(SICI)1099-1492(199704)10:2<73::AID-NBM448>3.0.CO;2-4
23. Borenstein M, Hedges LV, Higgins JPT, Rothstein HR. Random-Effects Model. In: *Introduction to Meta-Analysis.* John Wiley & Sons, Ltd; 2009:69-75. doi:10.1002/9780470743386.ch12
24. Minati L, Aquino D, Bruzzone MG, Erbetta A. Quantitation of normal metabolite concentrations in six brain regions by in-vivo ¹H-MR spectroscopy. *J Med Phys Assoc Med Phys India.* 2010;35(3):154-163. doi:10.4103/0971-6203.62128
25. Wright AM, Murali-Manohar S, Borbath T, Avdievich NI, Henning A. Relaxation-corrected macromolecular model enables determination of ¹H longitudinal T1-relaxation times and concentrations of human brain metabolites at 9.4T. *Magn Reson Med.* 2022;87(1):33-49. doi:10.1002/mrm.28958
26. Landheer K, Gajdosik M, Treacy M, Juchem C. Concentration and effective T-2 relaxation times of macromolecules at 3T. *Magn Reson Med.* 2020;84(5):2327-2337.
27. Hoefemann M, Bolliger CS, Chong DGQ, van der Veen JW, Kreis R. Parameterization of metabolite and macromolecule contributions in interrelated MR spectra of human brain using multidimensional modeling. *NMR Biomed.* 2020;33(9):e4328. doi:10.1002/nbm.4328
28. Cudalbu C, Behar KL, Bhattacharyya PK, et al. Contribution of macromolecules to brain ¹H MR spectra: Experts' consensus recommendations. *NMR Biomed.* 2021;34(5):e4393. doi:10.1002/nbm.4393
29. Provencher S. LCMoDel User's Manual. Accessed November 4, 2024. <http://s-provencher.com/lcm-manual.shtml>
30. Clarke WT, Bell TK, Emir UE, et al. NIfTI-MRS: A standard data format for magnetic resonance spectroscopy. *Magn Reson Med.* 2022;88(6):2358-2370. doi:10.1002/mrm.29418
31. McCarthy P. FSLeYes. Published online April 23, 2024. doi:10.5281/zenodo.11047709

32. Degaonkar MN, Pomper MG, Barker PB. Quantitative proton magnetic resonance spectroscopic imaging: Regional variations in the corpus callosum and cortical gray matter. *J Magn Reson Imaging*. 2005;22(2):175-179. doi:10.1002/jmri.20353
33. Emir UE, Auerbach EJ, Moortele PFVD, et al. Regional neurochemical profiles in the human brain measured by ¹H MRS at 7 T using local B1 shimming. *NMR Biomed*. 2012;25(1):152-160. doi:10.1002/nbm.1727

Supporting Information

Supporting Information Table S1: Example of the metabolite dataframe that is integrated in the MRS phantom.

Supporting Information Table S2: Computation times of all steps in the 3D MRS phantom framework.

Table S1: Example of the metabolite dataframe for two metabolites: ml and NAA. For each metabolite there are as many entries as labels that are used in the MRS Phantom. All values for WM and GM are based on the used literature study, CSF values are manually set, and all background values are set to 0.0. T₁ values are not added yet but have been implemented as placeholder for future updates.

Metabolite	Label	Tissue	Conc_mean [mM/IU]	Conc_std [mM/IU]	T ₁ [ms]	T ₂ [ms]
ml	0	Background	0.0	0.0	0.0	0.0
ml	1	WM	5.42	0.63	-	189.90
ml	2	GM	4.86	0.27	-	200.03
ml	3	CSF	-	-	-	-
NAA	0	Background	0.0	0.0	0.0	0.0
NAA	1	WM	8.76	1.1	-	291.44
NAA	2	GM	8.33	0.59	-	265.31
NAA	3	CSF	-	-	-	-

Table S2: Computation times of all steps in the 3D MRS phantom framework. Times are in seconds (s) and are given for both skeletons and tested resolutions.

Step	BigBrain-MR		MRiLab	
	1 mm	3 mm	1 mm	3 mm
Database filtering			2 s	
Generating phantom	181 s	11 s	253 s	7 s
Loading phantom	10 s	< 1 s	15 s	< 1 s
Spectral simulation for all slices (number of spectra)	2,087 s (1,657,384)	74 s (61,412)	2,532 s (1,955,621)	88 s (72,395)
Downsampling MRSI + saving NIfTI-MRS files	457 s	16 s	619 s	22 s